Journal of ELECTRICAL ENGINEERING, VOL. 59, NO. 3, 2008, 139–145

EXPERIMENTAL VERIFICATION OF CHATTERING FREE SLIDING MODE CONTROL OF THE DRIVE POSITION EMPLOYING PMSM

Ján Vittek * — **Stephen J. Dodds** ** — **Peter Briš** *
Marek Štulrajter * — **Pavol Makyš** *

A new position controller for electric drives employing PMSM is presented based on the principles of sliding mode control and respecting the principles of vector control. The proposed controller is designed to be free of chattering and therefore suitable for high precision applications and has a parallel control structure for independent control of the motor excitation current and the rotor angle. To eliminate control chattering a smoothing integrator is introduced into both parallel controllers and furthermore the switching boundary is replaced by a boundary layer. The simulations and experimental results indicate that the proposed control system exhibits the desired robustness and therefore warrants further development and investigation.

K e y w o r d s: electric drives, position control, PMSM, sliding mode control, observer

1 INTRODUCTION

Robustness is a desirable property of automatic control systems and is defined here as the ability to yield a specified dynamic response to its reference inputs despite uncertainties in the plant mathematical model and unknown external disturbances. In its basic form, sliding mode control (SMC) is known to achieve such robustness with respect to plant uncertainties [1], [2] and external disturbances [3], [4] too. Various forms of SMC have been applied to complex mechanical systems [5], [6] but the original contribution of this paper is a new structure of SMC applied to achieve both flux and position control of electric drives employing permanent magnet synchronous motors (PMSM) without control chatter [1]. The control system may be designed to yield a specified settling time of the step response. It also obeys a known closed loop transfer function and can therefore be used in conjunction with a derivative feed-forward pre-compensator to eliminate dynamic lag for high precision motion control applications.

Based on the principles of vector control, the PMSM is divided into two control channels for

a) indirect control of the magnetic flux using the direct axis stator voltage and current components as, respectively, the control input and controlled output, and
b) control of the rotor angle using the quadrature axis stator voltage component as the control input and the rotor angle measurement the controlled output.

The basic principles of SMC are applied to both of these channels yielding the parallel control structure of Figure 1.

Here, u_a, u_b, u_c and i_a, i_b, i_c are, respectively, the physical stator voltages and currents, i_d is the computed direct axis current component, $u_{d\,\mathrm{dem}}$, $u_{q\,\mathrm{dem}}$ are the direct and quadrature axis components of the computed stator voltage demands, which are the control variables, Γ is the machine torque developed by the rotor angle control loop. Γ_{Le} is the external load torque referred to the motor output shaft, $i_{d\,\mathrm{dem}}$ is the demanded direct axis current (*ie* the excitation current) achieving the required magnetic flux and $\Theta_{r\,\mathrm{dem}}$ is the demanded rotor angle.

To avoid control chatter, a smoothing integrator is introduced into both control channels in addition to the usual replacement of the signum function by a transfer characteristic consisting of a proportional high gain with saturation, which replaces the switching boundary by a boundary layer. Operation in the sliding mode implies operation on the linear, high gain characteristic of this transfer characteristic enabling rearrangement of the block diagrams (*valid for both control channels*) to avoid the extra output derivative that would be needed in a conventional sliding mode controller after insertion of the control smoothing integrator.

Although the smoothing integrators alone would, in principle, eliminate the control chatter, the finite sampling frequency of the digital processor would, in practice, yield zigzag variations in the control variables, $u_{d\,\mathrm{dem}}$ and $u_{q\,\mathrm{dem}}$, which might interact adversely with the power electronic switching (PWM in Fig. 1). To avoid this, the switching boundary is replaced by a boundary layer. This, in principle, also eliminates the control chatter, but alone would allow steady state errors with constant load torque components due to the finite gain within the boundary layer. Hence the two control chatter elimination methods are employed together to produce a better result than they could individually. The weighting coefficients of the SMC switching boundaries are chosen such that control of the direct axis stator current component, and

* University of Žilina, Faculty of Electrical Engineering, Univerzitná 1, 010 26 Žilina, Slovakia; jan.vittek@fel.uniza.sk ** University of East London, School of Computing and Technology, 4 University Way, E16 2RD London, United Kingdom; stephen.dodds@spacecom.co.uk

ISSN 1335-3632 © 2008 FEI STU

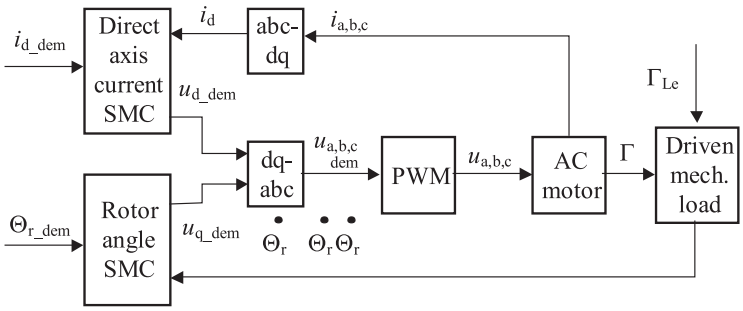

Fig. 1. Parallel control structure of proposed control system.

most importantly, position control of the PMSM rotor are achieved with specified step response settling times.

It should be noted that the structure of the third order rotor angle control loop of Fig. 1 is applicable to any single input, single output plant of rank, $r = 3$, and can easily be generalised to plants with other ranks.

Two approaches for obtaining estimates of the rotor angular velocity and acceleration, which are needed for the rotor angle control, are presented and discussed in the paper.

2 THE CONTROL ALGORITHMS

A. Sliding Mode Control Algorithm

In sliding mode control, only the plant rank, r, has to be known. In its basic form, SMC is a form of bang-bang state feedback control in which the control variable, u, switches between two limits and a simple form of sliding mode control [7] yielding robustness with respect to plant parameters and external disturbances, can be expressed in two parts defined by equations (1) and (2) following:

$$\boldsymbol{u} = -\boldsymbol{u}_{\max} \operatorname{sign}\left[S(\boldsymbol{y}, y_{\mathrm{dem}})\right] , \tag{1}$$

where $\boldsymbol{u}_{\max}$ is the control saturation limit imposed by the hardware and the switching function is defined as:

$$S(\boldsymbol{y}, y_{\mathrm{dem}}) = y - y_{\mathrm{dem}} + \sum_{i=1}^{r-1} w_i y^{(i)}, \tag{2}$$

where $\boldsymbol{y} = \left[y, \dot{y}, \ddot{y}, \ldots, y^{(r-1)}\right]^\top$ is a vector of state variables comprising the controlled output and its derivatives and r is the rank of the plant (*ie*, *the number of poles minus the number of zeros of the transfer function in the case of a linear plant*) and y_{dem} is the demanded value of y. The equation of the *switching boundary*:

$$S(\boldsymbol{y}, y_{\mathrm{dem}}) = 0 , \tag{3}$$

defines all points in the sub-state space, $\boldsymbol{y} = \left[y, \dot{y}, \ddot{y}, \ldots \right.$ $\left. \ldots, y^{(r-1)}\right]^\top$, at which switching of u take place. In the sliding mode, $S(\boldsymbol{y}, y_{\mathrm{dem}})$ is maintained almost zero and therefore the closed loop dynamics is almost entirely governed by equation (3) chosen by the control system designer, thereby achieving the required robust performance.

In ideal sliding motion the controller maintains the switching function zero, *ie*, $S(\boldsymbol{y}, y_{\mathrm{dem}}) = 0$ and the closed-loop system precisely follows the switching boundary and in view of equation (2), with $n = r - 1$, obeys:

$$y - y_{\mathrm{dem}} + \sum_{i=1}^{n} w_i y^{(i)} = 0 . \tag{4}$$

This is the *linear differential equation governing the behaviour of the closed-loop system*. Laplace transforms with zero initial conditions then yields:

$$\left[1 + \sum_{i=1}^{n} w_i s^i\right] y(s) = y_{\mathrm{dem}}(s) , \tag{5}$$

from which the closed-loop transfer function is:

$$\frac{y(s)}{y_{\mathrm{dem}}(s)} = \frac{1}{1 + w_1 s + w_2 s^2 + \cdots + w_n s^n} . \tag{6}$$

This is a form of the *general* transfer function of a linear system of order, n, with a d.c. gain of unity. The reason for the closed-loop system being of order, $n = r-1$, while the plant rank is r, is that in the sliding mode, the control system is forced to remain in the $n = r - 1$ dimensional switching boundary within the r-dimensional sub-state space [1].

The condition for sliding motion is that the point, $\boldsymbol{y}$, in the r dimensional sub-state space with components $y_{\mathrm{dem}}, y, \dot{y}, \ldots, y^{r-1}$, is driven back towards the switching boundary (2) from both sides by the designed control law. This is expressed mathematically as: . This condition will only be satisfied over a finite region of the switching boundary and, in general, this region may be increased in size by incresing the maximum control level $u_{\max}$.

Most importantly, the n weighting coefficients of the switching boundary may be chosen independently and this makes it possible to design the system by the method of *pole assignment*. If a specified settling time, T_s, is given for a control system and zero overshoot of the step response is required, then with n closed loop poles having

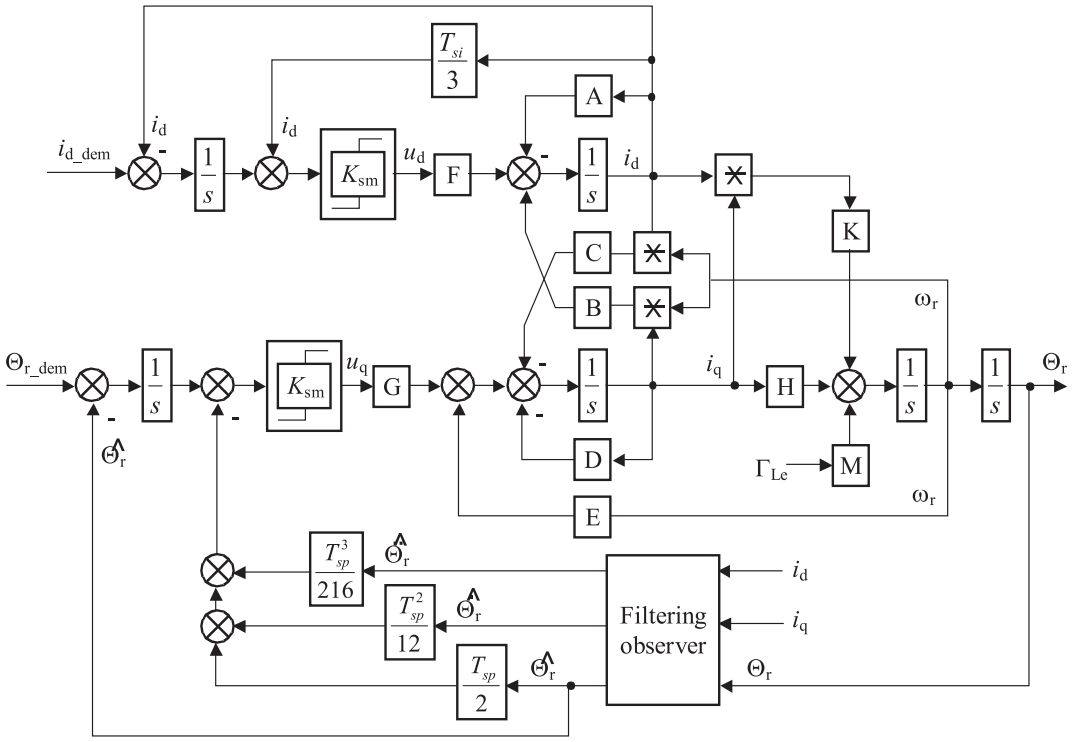

Fig. 2. Position controlled permanent magnet synchronous motor.

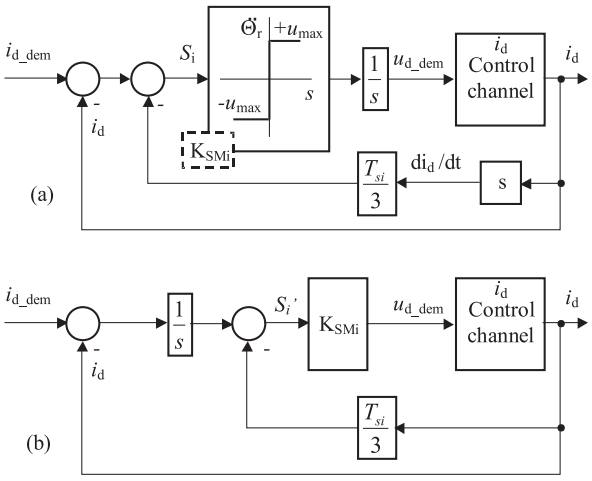

Fig. 3. Sliding mode control loop for id current component.

equal real parts $-1/T_c$, the following Dodds settling time formula [8] applies:

$$T_s = 1.5(1+n)T_c\,. \tag{7}$$

This yields the general transfer function

$$\frac{y(s)}{y_{\rm dem}(s)} = \left[\frac{1}{1+\frac{sT_s}{1.5(1+n)}}\right]^n. \tag{8}$$

The pole placement design is then carried out by expanding (8) and comparing coefficients with (6) to obtain design equations for the weighting coefficients, w_i, $i = 1, 2, \ldots, n$, in terms of T_s.

As far as the SMC theory is concerned the insertion of the smoothing integrator discussed in Section I to alleviate the harmful effects of control chatter essentially creates a 'new' plant comprising the original plant and the smoothing integrator. This new plant is of order 1 greater than the original and this therefore increases the order of the closed loop system by 1.

Now the SMC control algorithms for the PMSM position controlled drive and the supporting rotor angle derivative estimation algorithms will be fully derived and discussed.

First, the differential equations describing the PMSM are as follows:

$$\frac{{\rm d}\Theta_r}{{\rm d}t} = \omega_r\,, \tag{9}$$

$$\frac{{\rm d}\omega_r}{{\rm d}t} = (H + Ki_d)i_q - M\Gamma_{L_e}\,, \tag{10}$$

$$\frac{\rm d}{{\rm d}t}\begin{bmatrix} i_d \\ i_q \end{bmatrix} = \begin{bmatrix} -A & B\omega_r \\ -C\omega_r & -D \end{bmatrix}\begin{bmatrix} i_d \\ i_q \end{bmatrix} - E\omega_r + \begin{bmatrix} F & 0 \\ 0 & G \end{bmatrix}\begin{bmatrix} u_d \\ u_q \end{bmatrix}, \tag{11}$$

where, $A = R_s/L_d$; $B = pL_q/L_d$; $C = pL_d/L_q$; $D = R_s/L_q$; $G = 1/L_q$; $E = p\Psi_{PM}/L_q$; $F = 1/L_d$, $H = 3p\Psi_{PM}/(2J_r)$; $K = 3p(L_dL_q)/(2J_r)$ and $M = 1/J_r$.

Figure 2 shows the corresponding block diagram of the PMSM together with details of the SMC control loops for the excitation current and the rotor position.

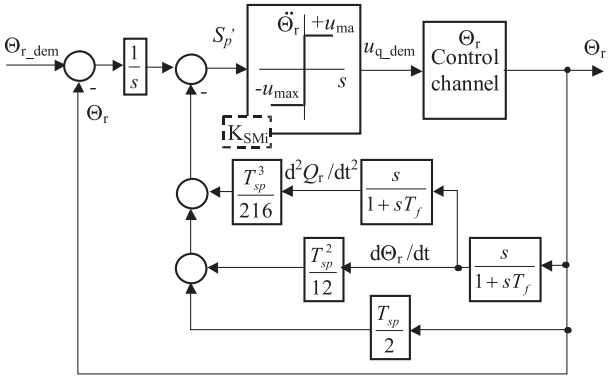

Fig. 4. Position controlled permanent magnet synchronous motor.

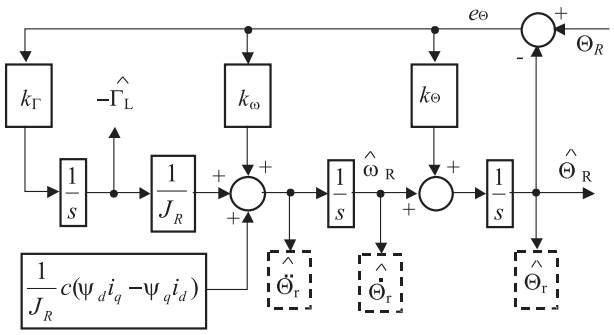

Fig. 5. Block diagram of observer.

The SMC theory introduced in Section 2 is now applied to the rotor angle and excitation current control channels outlined in Section 1 and evident in the mathematical representation of the PMSM in the rotor fixed frame defined by equations (9) to (11) and Fig. 2, resulting in the SMC algorithms also defined by Fig. 2. For control of the motor excitation current component, i_d, $y_{\rm dem} = i_{d\,\rm dem}$, $r = 2$ and $n = 1$ while for control of the rotor angle, Θ_r, $y_{\rm dem} = \Theta_{r\,\rm dem}$, $r = 4$ and $n = 3$ including the smoothing integrators.

Since the control channel for the excitation current, i_d, is of the rank $r = 2$, this SMC loop, in theory, needs the first current derivative and the switching function (2) becomes

$$S_i = i_{d\,\rm dem} - \Big(i_d + \frac{T_{si}}{3}\frac{{\rm d}i_d}{{\rm d}t}\Big), \tag{12}$$

as shown in Fig. 3a. In the sliding mode, however, the saturating transfer characteristic shown in Fig. 2 may be replaced by the high gain, K_{SMi}, in which case, the smoothing integrator effectively cancels the differentiator in the inner feedback loop resulting in the simplified block diagram of Fig. 3b. The resulting equation for the control variable is then:

$$u_{d\,\rm dem} = K_{SMi}S_i' = K_{SMi}\Big[\int \big(i_{d\,\rm dem} - i_d\big){\rm d}t - \frac{T_{si}}{3}i_d\Big] \tag{13}$$

from which for $S_i' \to 0$ is valid:

$$\frac{1}{s}\left[i_{d\,\rm dem}(s) - i_d(s)\right] - \frac{T_{si}}{3}i_d(s) \to 0$$

$$\Rightarrow \frac{i_d(s)}{i_{d\,\rm dem}s) = \frac{1}{1+T_{si}}/3}. \tag{14}$$

Since the control channel for the rotor position is of rank $r = 4$, in theory, according to (2), the first, second and third derivatives of position are required as feedback for the SMC algorithm, and switching function (2) becomes:

$$S_P = \Theta_{r\,\rm dem} - \Big(\Theta_r + \frac{T_{sp}}{2}\frac{{\rm d}\Theta_r}{{\rm d}t} + \frac{T_{sp}^2}{12}\frac{{\rm d}^2\Theta_r}{{\rm d}t^2} + \frac{T_{sp}^3}{216}\frac{{\rm d}^3\Theta_r}{{\rm d}t^3}\Big). \tag{15}$$

Following similar lines to the simplification of the excitation current SMC leading to Fig. 3b, however, the control smoothing integrator reduces orders of the derivative feedbacks by 1, meaning that only the first and second derivatives (*speed and acceleration*) are required. As switching function $S_P' \to 0$ the resulting position SMC law is

$$u_{q\,\rm dem} = K_{SMp}\Big[\int(\Theta_{r\,\rm dem} - \Theta_r){\rm d}t - \frac{T_{sp}}{2}\Theta_r - \frac{T_{sp}^2}{12}\dot\Theta_r - \frac{T_{sp}^3}{216}\ddot\Theta_r\Big]. \tag{16}$$

Figure 4 shows this version of the SMC loop in which the pure differentiations are combined with first order filters with time constant, T_f for avoiding amplification of high frequency components of measurement noise.

Non-zero T_f will impose an upper limit on K_{SMp} to maintain closed loop stability but if sufficiently small will not substantially affect the robustness. According to Fig. 4, as $S_p' \Rightarrow 0$

$$\frac{1}{s}\left[\big(\Theta_{r\,\rm dem}(s) - \Theta_r(s)\big)\right] = \Big(\frac{T_{sp}}{2} + \frac{T_{sp}^2}{12}s + \frac{T_{sp}^3}{216}s^2\Big)\Theta_r(s)$$

$$\Rightarrow \frac{\Theta_r(s)}{\Theta_{r\,\rm dem}(s)} = \Big[\frac{1}{1 + s(T_{sp}/6)}\Big]^3, \tag{17}$$

which is as required. So the individual feedbacks shown in Fig. 4 correspond to (16) in the time domain. In cases where the measurement noise imposes a longer filtering time constant, T_f, than required to retain the demanded robustness, then an alternative approach is to employ an observer for estimation position, speed and acceleration that has measurement noise filtering properties without the drawback of introducing a dynamic lag in the control loop. This, however, requires a plant state space model but since this is available in the drive under investigation, the observer solution is chosen for the simulations and corresponding experiments.

The SMC control laws derived in this section may be identified in Fig. 2.

B. Estimation of Rotor Speed and Acceleration

There are limits imposed on the control block diagram of Fig. 1, [5]. The bandwidth of the inner current control loop is limited due to the PWM. If the encoder is exploited it behaves like a sampler whose sampling frequency is proportional to and therefore reduces with speed. Hence the finite resolution of the shaft encoder for the rotor position measurement imposes a severe bandwidth limitation at low and near zero speeds which occur as the position control system settles with a constant reference input. This will severely impair the accuracy of the speed and acceleration estimation if simple software differentiation is used. The aforementioned observer could, however, help to alleviate this problem in view of the ability of the real time plant model to continue to produce time varying state estimates between the shaft encoder increments. For this investigation a type of observer developed previously for forced dynamic control (FDC) [8] is exploited. This is capable of producing a filtered estimate of the external load torque, Γ_{Le} as well as filtered estimates of the rotor position, speed and acceleration. Although the load torque estimate is not used directly by the SMC rotor position control loop, it is useful in avoiding steady state errors in the state estimates which would otherwise occur with constant components of the external load torque.

The load torque is treated as a state variable assuming that it is constant over a time interval that is short compared with the closed loop time constant, T_{sp}, of the position control loop. The real time plant model in the observer is therefore based on equations (9) and (10) augmented by a further state equation, $\mathrm{d}\Gamma_{Le}/\mathrm{d}t = 0$. The observer correction loop is actuated by the error, $e_\Theta = \Theta_R - \widehat{\Theta}_R$, between the measured rotor position and its estimate from the observer. The observer state equations are therefore as follows:

$$\frac{\mathrm{d}\widehat{\Theta}_r}{\mathrm{d}t} = \hat{\omega} + k_\Theta e_\Theta \,, \tag{18}$$

$$\frac{\mathrm{d}\hat{\omega}_r}{\mathrm{d}t} = \frac{1}{J_R}\left[c\big(\psi_d i_q - \psi_q i_d\big) - \widehat{\Gamma}_{Le}\right] + k_\omega e_\Theta \,, \tag{19}$$

$$\frac{\mathrm{d}\widehat{\Gamma}_{Le}}{\mathrm{d}t} = 0 + k_\Gamma e_\Theta \,. \tag{20}$$

The corresponding block diagram is shown in Fig. 5.

Here, k_Θ k_ω and k_Γ are the correction loop gains. Again with the aid of the settling time formula (7), design equations for these gains may be derived to yield a correction loop settling time, T_{so}, defined as the time taken for $|e_\Theta(t)|$ to fall to and stay below 5 % of its peak value following a disturbance. Hence, equating the desired characteristic polynomial (LHS of (21)) and the characteristic polynomial obtained from Fig. 4 using Mason's formula (RHS of (21)) yields the gain equations (22):

$$s^3 + \frac{18}{T_{so}}s^2 + \frac{108}{T_{so}^2}s + \frac{216}{T_{so}^3} = s^3 + s^2 k_\Theta + s k_\omega + \frac{k_\Gamma}{J_R} \,, \tag{21}$$

$$k_\Theta = \frac{18}{T_{so}}, \quad k_\omega = \frac{108}{T_{so}^2}, \quad k_\Gamma = \frac{216 J_R}{T_{so}^3} \,. \tag{22}$$

Although the load torque is assumed constant in the formulation of the real time model of the observer, the estimate of the load torque, $\widehat{\Gamma}_{Le}$, will follow a time varying load torque and will do so more faithfully as T_{so} is reduced. The filtered outputs of observer exploited in the simulations and experiments are shown in Fig. 5.

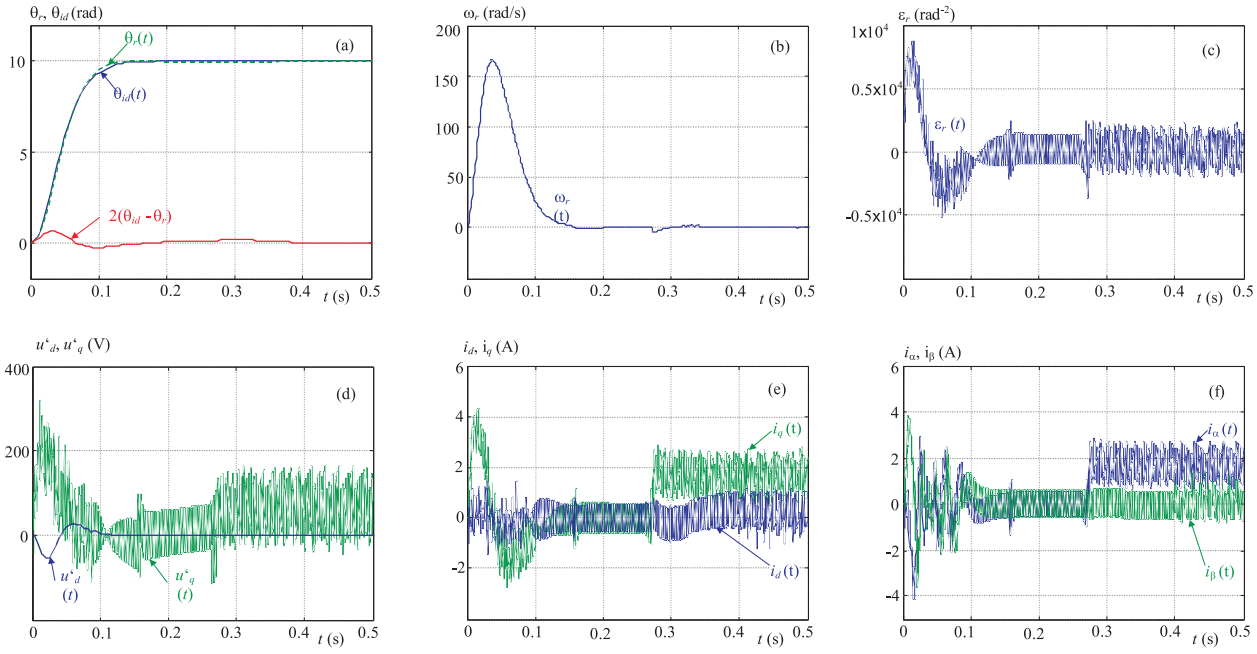

Fig. 6. Simulation results for SMC of rotor angle.

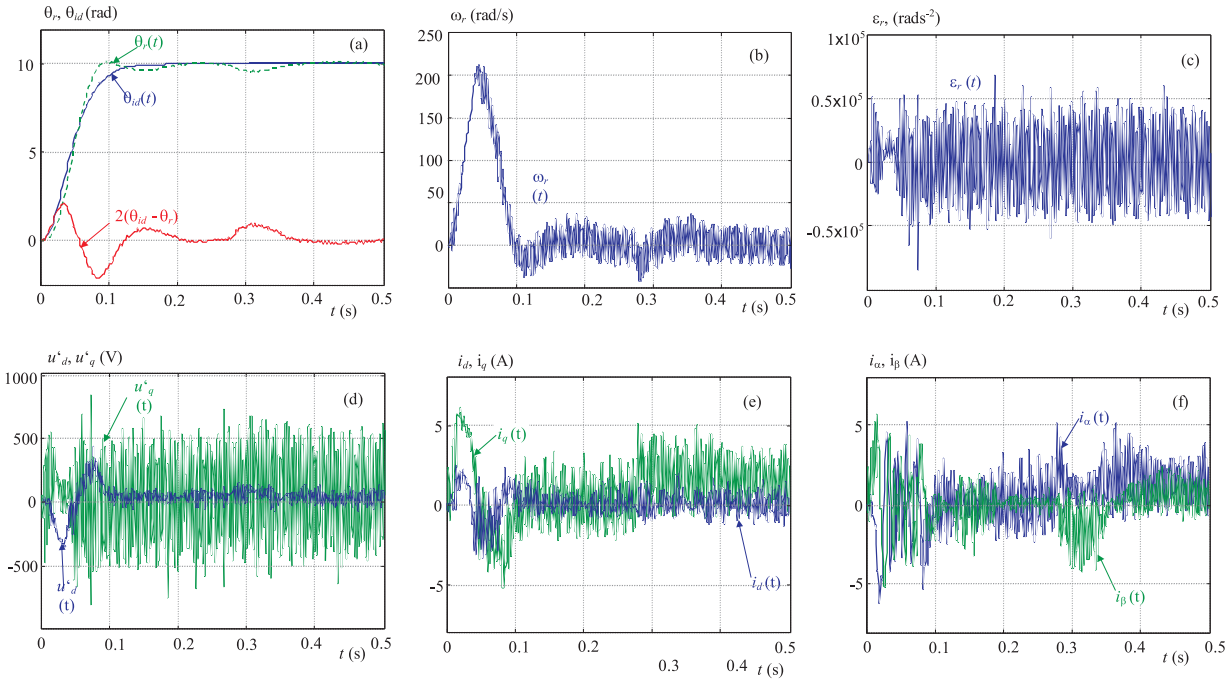

Fig. 7. Preliminary experimental results for SMC of rotor angle.

3 SIMULATIONS AND EXPERIMENTAL VERIFICATION

The simulation and subsequent experimental results for control of the PMSM rotor angle are presented in Fig. 6 and Fig. 7, respectively. The parameters of the PMSM relevant to both simulation and experiments are listed in [7].

For the simulations the computational step is $h = 1e-4s$, which corresponds to the sampling frequency achieved during a previous digital implementation of the algorithms for SMC of the speed of a PMSM drive. The simulations are carried out with zero initial state variables and a step rotor position demand, $\Theta_{r\,\mathrm{dem}}$, equal to 10 radians and a prescribed settling time of $T_s = 0.1$ s. In the simulations a step external load torque of 2 Nm (*ie*, 1.5 *of the PMSM nominal torque*) is applied at $t = 0.27$ s, being zero for the time interval $t < 0.27$ s. The settling time of the load torque observer is chosen as $T_{so} = 10$ ms. The settling time of the current, id control loop is chosen as $T_{so} = 20$ ms.

Subplot (a) shows the response of the control system together with the ideal response computed from transfer function (17) to a step position demand of $\Theta_{r\,\mathrm{dem}} = 10$ rad including the 2 times magnified difference between them. Subplot (b) and subplot (c) show the rotor speed and angular acceleration as the outputs of the filtering observer taken as the inputs of control algorithm (16) for whole measure period. Applied stator voltages as a function of time are shown in subplot (d). Subplot (e) and subplot (f) show stator currents in d_q frame coupled to the rotor and α_β frame fixed to the stator of the machine respectively.

The experimental results of the rotor angle SMC (*for the idle running PMSM*) are shown in Fig. 7 in order corresponding to the previously presented simulations. The locked torque of the induction motor was applied at $t = 0.27$ s as load torque.

The motion of the corresponding state trajectory in the theoretical switching surface designed from transfer function (15) obtained from the aforementioned simulations and the corresponding state trajectory in the real switching surface obtained from the experiments are shown in Fig. 8.

Comparison of both, simulation and experimental results show a good agreement with the theoretical predictions made during the control law development. It is also evident that in the experiments as well as in the simulations, the rotor angle reaches 9.5 radians (95 % of demanded value) at a time very close to the prescribed settling time of 0.1 s. It can be therefore concluded that chattering free SMC of the electric drive with PMSM respecting vector control principles was verified not only with simulations but also experimentally.

4 CONCLUSIONS AND RECOMMENDATIONS

The chattering free control system for position control of the rotor of electric drive with PMSM based on the principles of SMC has been presented and verified by simulations and by experiments.

The simulation of the SMC algorithm for the external load torque of $\Gamma_{L\,\max} = 2$ Nm (*more than* 1.5 *of nominal torque*) show its very effective compensation and consequential robustness of the proposed control system to this disturbance. This implies also successful operation of the observer including the estimation not only of the load torque but also both derivatives of position (angular

speed and acceleration) needed by the position SMC algorithm. Further investigations should be carried out with regard to the dynamic changes of motor and load parameters to investigate the robustness and possibly use the load torque estimate, as in the forced dynamic control [8] in a modified SMC law with aim of improving the robustness further.

The precision of the SMC of the PMSM rotor angle might be further improved by adding a precompensator control loops or an outer model reference adaptive control loop because of known prescribed behavior of the control system.

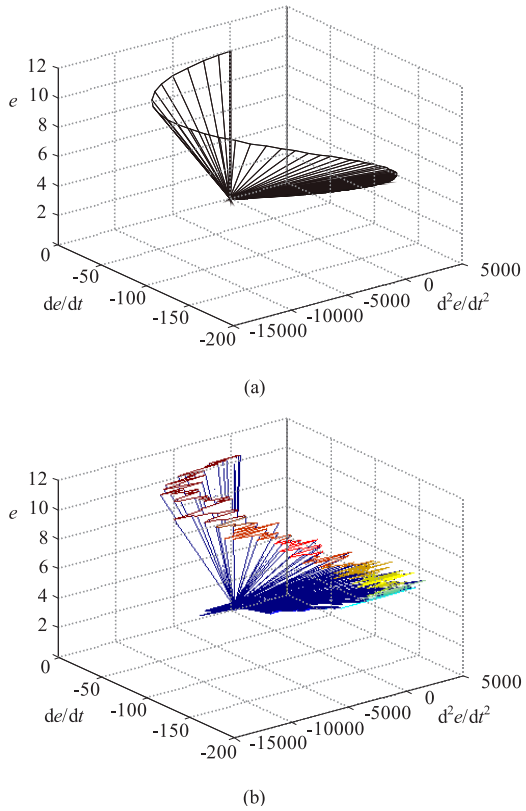

Fig. 8. Prescribed and achieved position switching surface.

Acknowledgment

The authors wish to thank Slovak Grant Agency VEGA for funding the project No. 4087/07 'Servosystems with Rotational and Linear Motors without Position Sensor'.

References

[1] UTKIN, V. I.: Sliding Modes in Control and Optimisation, Springer-Verlag, Berlin, 1992.

[2] AGUILAR, O.—LOUKIANOV, A. G.—CANEDO, J. M.: Observer-Based Sliding Mode Control of Synchronous Motor, IFAC Congress on Automatic Control proc., Guadalajara, Mexico 2002, CD-Rom.

[3] URLEP, E.—JEZERNIK, K.: Speed Sensorless Variable Structure Control of PMSM, IEEE IECON 2006 conf. proc., Paris, France, 2006, pp. 1194–1199.

[4] BROCK, S.—DESKUR, J.—ZAWIRSKI, K.: Robust Speed and Position Control of PMSM Using Modified Sliding Mode Method, EPE-PEMC 2000 conf. proc., vol. 6, Košice, Slovakia, pp. 6-29-6-34.

[5] BRANDTSTADTER, H.—BUSS, M.: Control of Electromechanical Systems Using Sliding Mode Techniques, CDC-EEC 2005 conf. proc., Sevilla, Spain, CD-Rom.

[6] RYVKIN, S.—IZOSIMOV, D.—PALOMAR-LEVER, E.: Digital Sliding Mode Based References Limitation Law for Sensorless Control of an Electromechanical Systems, Journal of Physics, IOP Publ. Ltd, series **23** (2005), 192–201.

[7] DODDS, S. J.: Handbook for MSc. Computer Control Module EEM114, (unpublished but available upon application), University of East London, School of Computing and Technology, UK.

[8] DODDS, S. J.: Settling Time Formulae for the Design of Control Systems with Linear Closed Loop Dynamics, Proceedings of the Third Annual Conference on Advances in Computing and Technology, AC&T2008,, pp. 31–39.

[9] VITTEK, J.—DODDS, S. J.: Forced Dynamics Control of Electric Drives, bilingual scientific monograph, EDIS, Žilina University Publishing Centre, 2003, http://www.kves.uniza.sk, (E-learning)..

[10] KORONDI, P.—HASHIMOTO, H.—UTKIN, V. I.: Direct Torsion Control of Flexible Shaft in an Observer-Based Discrete Sliding Mode, IEEE Trans. on Industrial Electronics **45** No. 2 (1998), 291–296.

[11] RYAN, E. P.: Optimal Relay and Saturating Control System Synthesis, Peter Peregrinus, 1982.

[12] COMNAT, V.—CERNAT, M.—MOLDOVEANU, F.—UNGAR, R.: Variable Structure Control of Surface Permanent Magnet Synchronous Machine, Proceedings of PCIM'99 conferenc, Nurnberg, Germany, 1999, pp. 351–356.

[13] GYEVIKI, J.—TOTH, I. T.—ROZSAHEGYI, K.: Sliding Mode Control and its Application on an Servo-Pneumatic Positioning System, Transactions on Automatic Control and Computer Science **49** (2004), University of Timosoara, Romania.

[14] KORONDI, P.: Tensor Product Model Transformation-Based Sliding Surface Design, Acta Polytechnica Hungarica **3** No. 6 (2006), 23–35.

[15] ZILKOVA, J.—TIMKO, J.—GIROVSKY, P.: Nonlinear System Control Using Neural Networks, Acta Polytechnica Hungarica **3** No. 4 (2006), 85–94.

[16] BOLDEA, I.—NASAR, A. S.: Vector Control of AC Drives, CRC Press, London, 1992.

[17] BELAI, I.—ZALMAN, M.: Predictive Current Controller of the Vector Controlled Asynchronous Motor, Journal of Electrical Engineering **48** No. 07-08 (1997), 201–204.

[18] PERDUKOVA, D.—FEDOR, P.—TIMKO, J.: Modern Methods of Complex Drives Control, Acta Technica CSAV **49** (2004), 31–45.

[19] KARDOS, J.: Theory of Systems with Variable Structure and Time-Suboptimal Position Control, HMH and AT&P Press, Bratislava, 2007. (in Slovak)

Received 8 December 2007

Ján Vittek is professor of the Faculty of Electrical Engineering, University of Žilina, Univerzitná 1, 010 26 Žilina, Slovakia.

Stephan J. Dodds is professor of the School of Computing and Technology, University of East London, 4-6 University Way, London E16 2RD, United Kingdom.

Peter Brišš is postgraduate student in Power Electrical Engineering of the Faculty of Electrical Engineering, University of Žilina.

Pavol Makýš and **Marek Štulrajter** are researchers with the Faculty of Electrical Engineering, University of Žilina.